VOL. 21, NO. 10, MAY 2026 ISSN 1819-6608
ARPN Journal of Engineering and Applied Sciences
©2006-2026 Asian Research Publishing Network (ARPN). All rights reserved.
www.arpnjournals.com

RELATIVISTIC PERSPECTIVES On $e^{\pm}$ IMPACT IONIZATION OF HYDROGEN (2S) IN SYMMETRIC COPLANAR GEOMETRIES

S. Banerjee and S. Dhar
Department of Mathematics, Chittagong University of Engineering and Technology (CUET), Chittagong-4349, Bangladesh
E-Mail: sushmita@cuet.ac.bd

ABSTRACT

In the higher-order Born approximation and within a symmetric coplanar geometry, we analytically calculate the triple differential cross sections (TDCSs) for electron and positron impact ionization of atomic hydrogen with its metastable 2S state, considering both low and high energy regimes. This is done for hydrogen atoms for incident electron energies of 250 eV and 511002 eV. The final state wave function is described using multiple scattering theory. The results reveal several intriguing characteristics. Relativistic and spin effects affect the triple differential cross sections. Due to the absence of theoretical models and data from experiments on this process, we are currently unable to validate our model against the findings. However, we believe that our work will provide a valuable foundation for future experimental and theoretical research in this area.

Keywords: relativistic, hydrogen atom, electron impact, positron impact, cross-sections, scattering.

Manuscript Received 1 April 2026; Revised 29 April 2026; Published 20 July 2026

1. INTRODUCTION

The interaction between charged particles and atoms is a fundamental problem in atomic and molecular physics [1-3]. Electron and positron impact ionization cross-sections are used in various research areas such as fusion physics, plasma physics, and space physics by various techniques, etc. [4-6]. Ionization cross-sections caused by electron and positron impact are also essential in atmospheric physics, radiation technology, astrophysics, etc. [7]. Ionization of the hydrogenic atom by an electron is a good representation of perturbation theory [8]. The experiments provide a clear concept of the kinematics of collisions by providing information regarding the path of the scattered and ejected electrons. A multiple scattering wave function with higher order and correlation effects was developed for two electrons moving in a Coulomb field. Hydrogen ionization by electron and positron scattering presents an intriguing system for evaluating theoretical methods due to its simplicity. Here, atomic hydrogen is selected for the excited state 2s as the target to focus on the collision process.

An atom can enter excited states by receiving more energy (for example, by the absorption of a sufficiently energetic photon) so that the electron can move into an excited state. The theoretical [9-24] and experimental [25-28] studies of electron and positron impact ionization collisions on various cross-sections have grown increasingly interesting for both ground state [8-14] and metastable state [15-20]. Following Das and Seal's [9] and Das and Dhar's wave function [28], many works have been done earlier [11], [15], [16], [17], [18], [19], [20] for non-relativistic as well as for relativistic atomic ionization. From an experimental as well as a theoretical perspective, the study of this process is significant and has applications in many contemporary areas of interest.

To our knowledge, there have been no experimental studies on the TDCS for ionization of metastable hydrogen atoms in 2S states by relativistic electrons and positrons with intermediate and high energies. The TDCS of metastable 2S state hydrogen atoms have not been theoretically estimated for relativistic purposes. Therefore, experimental results for H(2S) ionization will be valuable, and our findings will bring a new dimension to this field of study, both theoretically and experimentally. The current study significantly used the Lewis integral [29] for analytical calculation. This integral is frequently encountered in studies of atomic, molecular, nuclear, and plasma physics. These integrals appear naturally when two or more centers of force are present, and relative coordinates of the interacting particles are involved. The work explores the following issues to highlight:

a) Derivation of the First Born (FB) Triple differential cross section for ionization of a hydrogen atom by electron impact under various kinematic conditions.
b) Derivation of the Triple differential cross section for ionization of a hydrogen atom by electron and positron impact under various kinematic conditions.
c) The aim of conducting such a study is also to gather precise information about the similarities or dissimilarities between particle-matter and antiparticle-matter interactions.

The current findings are compared with other theoretical results [21]. The paper is organized as follows: Section 2 presents the theory of the existing research study. Section 3 concisely reviews the configurations of the present TDCS results for the electron and positron

©2006-2026 Asian Research Publishing Network (ARPN). All rights reserved.

impact ionization of H for the 2s state, and subsection 3.1, ionization mechanism, discusses the origin of each scattering amplitude from the transition matrix element, while subsection 3.2 presents the proposed direction for future research. Finally, in Section 4, we conclude by providing a summary and outlining future goals.

2. MATERIALS AND METHODS

We employ Das and Dhar's multiple scattering model [28], which focuses on calculating the energy spectrum of scattered electrons during K-shell ionization of silver atoms. Their model integrates relativistic effects in coplanar geometry and employs appropriate spinors for the final state. This approach, rooted in multiple scattering theory, offers a robust framework for studying atomic ionization, providing detailed and flexible insights into complex interactions. We derive the symmetric TDCSs for a hydrogen atom impacted by an electron, focusing on angular distributions. Additionally, we calculate TDCSs for the same atom by a positron. Studying these cross-sections helps us better understand how charged particles ionize, providing insights into fundamental atomic interactions. Figure 1 shows the layout of a coplanar (e, 2e) experiment, using clear symbols to help us understand atomic collisions and the path of electrons. The mathematical formulation is given below.

Let us begin by considering the single ionization process of a hydrogen atom:

$$H + e^- \rightarrow H^+ + 2e^-, \quad (1)$$

Where H represents a neutral hydrogen atom e^- is an incoming (incident) electron. H+ represents a hydrogen positive ion, and 2e- indicates the two outgoing electrons: one is ejected, and another is a scattered electron.

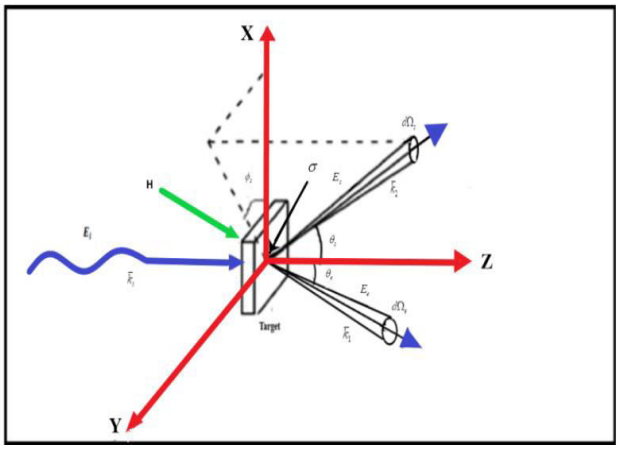


Figure-1. Diagrammatic representation of a coplanar (e, 2e) experiment.

In an (e, 2e) reaction, when an incident electron with momentum $\bar{k}_i$ and energy E_i collides with the target, it produces two electrons. These electrons have energies. E_e and E_s with momenta $\bar{k}_1$ and $\bar{k}_2$, and they are emitted into the solid angles $d\Omega_e$ and $d\Omega_s$ centered around the directions (θ_e, φ_e) and (θ_s, φ_s).

The component of the transition matrix for the ionization of hydrogen atoms by electrons, as described by Das and Seal [9], can be taken

$$T_{FI} = \left\langle \psi_f^{(-)}(\bar{r}_{ae}, \bar{r}_{pe}, \sigma_i', \sigma_f') \middle| V_i(\bar{r}_{ae}, \bar{r}_{pe}) \varphi_i(\bar{r}_{ae}, \bar{r}_{pe}, \sigma_i, \sigma_f) \right\rangle \quad (2)$$

Here, $\bar{r}_{ae}$ and $\bar{r}_{pe}$ represent the position vectors of the atomic electron and the projectile electron. (σ_i, σ_f) and (σ'_i, σ'_f) are the spin coordinates in the initial and final states of the two electrons.

Where the perturbation potential $V_i(\bar{r}_{ae}, \bar{r}_{pe})$ is given by

$$V_i(\bar{r}_{ae}, \bar{r}_{pe}) = \frac{\alpha_0}{r_{ab}} - \frac{\alpha_0 Z_{eff}}{r_b} \quad (3)$$

where z_{eff} denotes the effective nuclear charge, α_0 represents the fine structure constant, r_a and r_b are the distances of the two electrons from the nucleus and r_{ab} is the distance between them.

The initial channel unperturbed wave function is given in the following form

$$\Phi_i(\bar{r}_{ae}, \bar{r}_{pe}, \sigma_i, \sigma_f) = \frac{e^{ik.\bar{r}_b}}{(2\pi)^{3/2}} u_{\sigma_i}(0) u_{\sigma_f}(k_i) \varphi_{2s}(\bar{r}_{ae}) \quad (4)$$

$$\varphi_{2s}(\bar{r}_{ae}) = \frac{1}{4\sqrt{2\pi}} \left(2 - \bar{r}_{ae}\right) e^{-\lambda_1 r_{ae}} \quad (5)$$

Here, $\lambda_1 = \frac{1}{2}$, $\varphi_{2s}(\bar{r}_{ae})$ is the hydrogenic 2s-state wave function and the final-state wave function $\Psi_f^{(-)}(\bar{r}_{ae}, \bar{r}_{pe}, \sigma_i', \sigma_f')$ is given in

©2006-2026 Asian Research Publishing Network (ARPN). All rights reserved.

$$\psi_f^{(-)}(\bar{r}_{ae},\bar{r}_{pe},\sigma_i',\sigma_f') = A(\bar{k}_1,\bar{k}_2)\left[\varphi_{\bar{k}_1}^{(-)}(\bar{r}_{ae})e^{i\bar{k}_2.\bar{r}_{pe}} + \varphi_{\bar{k}_2}^{(-)}(\bar{r}_{pe})e^{i\bar{k}_1.\bar{r}_{ae}} + \varphi_{\bar{k}}^{(-)}(\bar{r})e^{i\bar{k}.\bar{R}} - 2e^{i\bar{k}_1.\bar{r}_{ae}+i\bar{k}_2.\bar{r}_{pe}}\right] u_{\sigma_i'}(\bar{k}_1)u_{\sigma_f'}(\bar{k}_2)/(2\pi)^3 \quad (6)$$

Here $A(\bar{k}_1,\bar{k}_2)$ is the normalization constant, and $u(\bar{k})$ represent Dirac free-particle spinors.
Where

$$\bar{r} = \frac{\bar{r}_{pe}-\bar{r}_{ae}}{2}, \bar{R} = \frac{\bar{r}_{pe}+\bar{r}_{ae}}{2}, \bar{k} = \frac{\bar{k}_2-\bar{k}_1}{2}, \bar{K} = \frac{\bar{k}_2+\bar{k}_1}{2}, \quad (7)$$

By applying Eqs. (3), (4) and (6) into Eq. (2), one formulates the following equations:

$$T_{FI} = \left(T_b + T_{b'} + T_i - 2T_{pb}\right)M_i M_f \quad (8)$$

where

$$T_b = \left\langle \varphi_{\bar{k}_1}^{(-)}(\bar{r}_{ae})e^{i\bar{k}_2.\bar{r}_{pe}} \middle| V_i \middle| \Phi_i\left(\bar{r}_{ae},\bar{r}_{pe},\sigma_i,\sigma_f\right)\right\rangle \quad (9)$$

$$T_{b'} = \left\langle \varphi_{\bar{k}_2}^{(-)}(\bar{r}_{pe})e^{i\bar{k}_1.\bar{r}_{ae}} \middle| V_i \middle| \Phi_i\left(\bar{r}_{ae},\bar{r}_{pe},\sigma_i,\sigma_f\right)\right\rangle \quad (10)$$

$$T_i = \left\langle \varphi_{\bar{k}}^{(-)}(\bar{r})e^{i\bar{K}.\bar{R}} \middle| V_i \middle| \Phi_i\left(\bar{r}_{ae},\bar{r}_{pe},\sigma_i,\sigma_f\right)\right\rangle \quad (11)$$

$$T_{pb} = \left\langle e^{i\bar{k}_1.\bar{r}_{ae}+i\bar{k}_2.\bar{r}_{pe}} \middle| V_i \middle| \Phi_i\left(\bar{r}_{ae},\bar{r}_{pe},\sigma_i,\sigma_f\right)\right\rangle \quad (12)$$

and $M_i = u^{\dagger}_{\sigma_i'}(k_1)u_{\sigma_i}(0)$ (13)

$$M_f = u^{\dagger}_{\sigma_f'}(k_2)u_{\sigma_f}(k_i) \quad (14)$$

The scattering amplitude may be represented in the following way.

$$f(\bar{k}_1,\bar{k}_2) = A(\bar{k}_1,\bar{k}_2)[\, f_{eT} + f_{PT} + f_{Pe} - 2f_{PWB}\,] \quad (15)$$

Here, f_{eT}, f_{PT}, f_{Pe}, and f_{PWB} are the amplitudes corresponding to the four terms of equation (6).

In this case of electron impact ionization, the values of the parameters α_1, α_2 and α are given below:

$$\alpha_1 = \frac{\alpha_0 Z_{eff}}{k_1} \text{ for } \bar{q} = \bar{k}_1, \ \alpha_2 = \frac{\alpha_0 Z_{eff}}{k_2} \text{ for } \bar{q} = \bar{k}_2 \text{ and } \alpha = -\frac{\alpha_0 Z_{eff}}{k} \text{ for } \bar{q} = \bar{k}\ \} \quad (16)$$

For positron impact ionization,

$$\alpha_1 = \frac{\alpha_0 Z_{eff}}{k_1} \text{ for } \bar{q} = \bar{k}_1, \ \alpha_2 = -\frac{\alpha_0 Z_{eff}}{k_2} \text{ for } \bar{q} = \bar{k}_2 \text{ and } \alpha = \frac{\alpha_0 Z_{eff}}{k} \text{ for } \bar{q} = \bar{k}\ \} \quad (17)$$

The direct scattering amplitude $f(\bar{k}_1,\bar{k}_2)$ is then determined from

$$f(\bar{k}_1,\bar{k}_2) = -(2\pi)^2 T_{FI} \quad (18)$$

The multiple scattering model [28] used calculations based on the Transition (T) matrix. However, this study improves upon the approach by employing the Scattering (S) matrix to accurately calculate several differential cross-sections. The S-matrix is preferred because it includes all possible final states and ensures that the sum of probabilities of all possible outcomes equals 1. On the other hand, the T-matrix only describes the interaction part and may not fully capture the transition amplitudes needed for accurate ionization cross-sections. The direct scattering S-matrix component is given by the relation [30]

$$S_{FI} = 1 - 2\pi i T_{FI} \quad (19)$$

Here, S_{FI} represents the scattering matrix, while T_{FI} denotes the transition matrix.

The triple differential cross-sections for the direct scattering matrix component are given by

$$\frac{d^3\sigma}{d\Omega_e d\Omega_s dE} = \frac{r_0^3 k_1 k_2 E_e E_s E_i}{k_i (2\pi)^3 \alpha_0^2}\overline{|S_{FI}|^2} \quad (20)$$

where r_0 is the electron's radius. For computational work, we used the MATLAB language for computer programming.

3. RESULTS AND DISCUSSIONS

In the present investigation, various cross-sections for ionization of the H atom by electron and positron in the symmetric geometry have been reported. The energy range is 250 eV$\leqslant Ei \leqslant$ 511002 eV. The presented findings on TDCS by electron and positron impact are compared with the existing theoretical assumptions.

For various kinematic conditions, the ionization of H(2s) states by relativistic electron and positron impact is presented. The attained new results are compared with the theoretical calculations of Jakha *et al*. [21]. Figure-2 shows the difference between the S-matrix and T-matrix for TDCS. In Figure-3, the slow electron scattering angle θ_e is considered the horizontal axis, ranging from 30 to 60 degrees and 40 to 50 degrees, whereas TDCS is plotted on the vertical axis. The obtained results correspond to Figure-3(a), with incident energy (E_i) of 250 eV and slow electron energy (E_e) of 123.3 eV. For Figure-3(b), the

©2006-2026 Asian Research Publishing Network (ARPN). All rights reserved.

incident energy is 3250 eV, and the slow electron energy is 1623.3 eV. In addition, Figure-3(c) pertains to incident energy of 4250 eV and a slow electron energy of 2123.3 eV. Similarly, the results obtained are related to Figure-4(a), with an incident energy (E_i) of 10000 eV and a slow electron energy of 4998.3 eV. Figure-4(b) corresponds to an incident energy of 15000 eV and slow electron energy of 7498.3 eV. Moreover, Figure-4(c) is associated with incident energy of 20000 eV and a slow electron energy of 9998.3 eV, while Figure-4(d) entails incident energy of 511002 eV and a slow electron energy of 255499.3 eV.

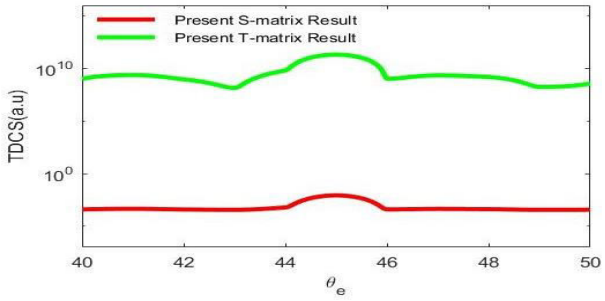


Figure-2. Cross sections of H(2s) scattering derived from S-matrix and T-matrix at E_i= 4250eV, E_e = 2123.3 eV. Theory: Red and green solids represent the present electron calculations using the S-matrix and T matrix respectively.

Figure-2 illustrates the comparison of the TDCS curve between the S-matrix and T-matrix derivations. The values of cross-section (TDCS) derived from the S-matrix are accurate due to the inclusion of the full scattering amplitude. It is notable that, in symmetric geometry, the curves from the scattering S-matrix display much lower TDCS values in comparison to those obtained from the T-matrix. This points to the constructive impact of the destructive interference effects captured by the S-matrix. The S-Matrix curve shows small cross sections in magnitude (about10^{-6} a.u.) due to the relationship between the T-matrix and S-matrix, as given in equation (19). Additionally, the inclusion of symmetry constraints and final-state interactions effectively reduces the probability of scattering events in symmetric geometries. The S-matrix also actively enforces unitarily and provides a more accurate treatment of exchange effects, resulting in smaller cross-section values. Conversely, the T-matrix consistently generates larger cross-sections in symmetric geometries due to its limitations in capturing interference and exchange effects.

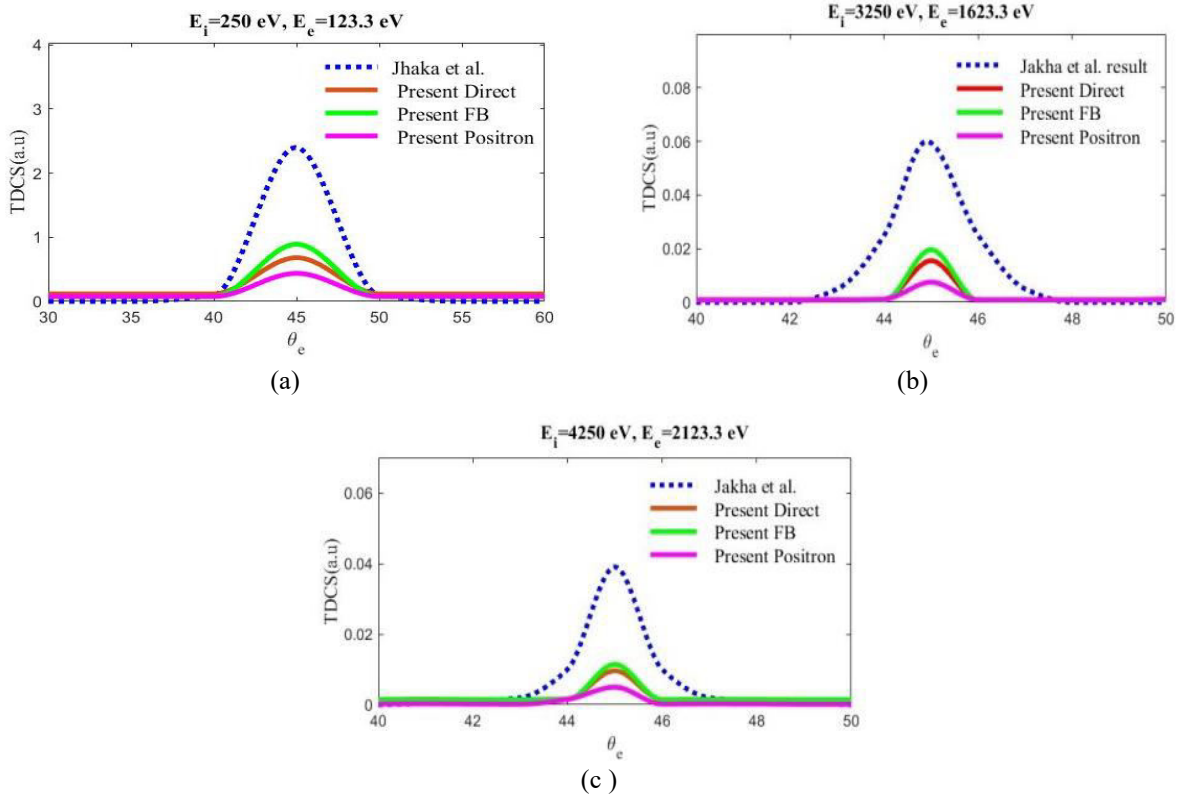


Figure-3. TDCS for e± H(2s) scattering at (a) E_i= 250eV, E_e = 123.3eV (b) E_i = 3250eV, E_e = 1623.3eV, (c) E_i= 4250eV, E_e = 2123.3eV. Theory: (-), the present electron calculations; (-), the present FBA result, (-) the present positron, blue short dash (---), Jakha *et al*. result [21].

Figure-3 (a) illustrates the triple differential scattering cross-section variation for fixed incident and ejected kinetic energy values, with E_i = 250 eV and E_e = 123.3 eV. The TDCS curve for electron scattering on the

©2006-2026 Asian Research Publishing Network (ARPN). All rights reserved.

H atom aligns with the theoretical calculations of Jakha *et al*. [21] since the metal studied is the same. Our curve exhibits a peak at an ejected angle of around 45 degrees. Current FB has a higher magnitude than the direct result due to the consideration of the first term of the amplitude, as well as the First Born approximation obeys with plane wave, which gives a higher magnitude. On the other hand, the present direct results deal with the Coulomb wave, which gives small magnitudes.

The electron scattering TDCS curve, which is shown in Figure-3(b), gives the same pattern in the whole region except at 43^0 and $47^{0,}$ with the result of Jakha *et al*. [21]. Due to the structure of the 2S wave function, especially near the node, and spin polarization effects in the relativistic treatment. In comparison, the peak of the current positron and FB results display almost similar patterns with different magnitudes. The present electron configuration, as shown in Figure-3(c), demonstrates a peak similar to the theoretical calculations of Jakha *et al*. [21], but shifted to the left. The shapes of the current FB and positron curves exhibit almost identical patterns but with differing magnitudes. The First Born (FB) and positron impact ionization are similar because both processes are governed by the same type of transition matrix element. In each case, the transition amplitude consists solely of the direct interaction term.

However, the difference in magnitudes reflects larger physical differences. The relativistic positron model used incorporates complete relativistic corrections, including spin effects that are not fully present in the simplified FB.

The relativistic symmetric triple differential cross section (TDCS) for ionization of the hydrogen atom in the 2S state by an electron tends to be higher than that by a positron due to the nature of the interactions between the incident particle (electron or positron) and the hydrogen atom. Several factors play a role within the relativistic regime. At relativistic energies, the incident electron moves at a very high velocity, and the repulsive Coulomb interaction helps focus the energy transfer directly into ionizing the 2S electron. This focused energy transfers and increased interaction in the spatial regions with high electron probability density lead to higher ionization probabilities and, therefore, a higher triple differential cross section (TDCS). On the other hand, Positrons (positively charged) experience the opposite interaction compared to electrons. Instead of being repelled by the bound 2S electron, the positron is attracted to it. This attractive force can result in the positron being pulled toward regions of lower electron probability, such as the radial node or closer to the nucleus, where the ionization probability is lower. The positron might get trapped in regions with less effective overlap with the electron's wave function, reducing the likelihood of direct ionization. As a result, the positron's interaction with the 2S electron is less direct and less focused on regions where ionization is most probable, leading to a lower TDCS than for electrons.

Figure-4 (a) depicts the variation of the triple differential scattering cross-section for a fixed incident energy and ejected kinetic energy value, E_i = 10000 eV, E_e = 4998.3 eV. Our TDCS curve for electron scattering on the H atom aligns with the theoretical calculations of Jakha *et al*. [21]. However, it is slightly shifted to the right at an ejection angle of approximately 44.7^0 and to the left at an ejection angle of around 45.5^0. This shift is due to relativistic wave functions and spin interactions, which influence the phase structure of the matrix elements. The current FB has a higher magnitude than the direct result due to the consideration of the first term of the amplitude.

The present electron scattering TDCS curve shown in Figure-4(b) overlaps in the recoil from 43^0 to 44^0 with the result of Jakha *et al*. [21]. In comparison, the present direct, FB, and positron results display a peak at an ejected angle of around 45^0, with the result of Jakha *et al*. [21], but shifted left with a different magnitude.

Present direct, FB, and positron configurations show a peak in Figure-4(c) similar to the theoretical calculations of Jakha *et al*. [21] but with a flatter form. This behavior is attributed, possibly due to using the same atomic states across models, to different forms of the transition matrix. The current electron scattering TDCS curve, as depicted in Figure-4(d), has a shape that closely resembles the findings of Jakha *et al*. [21] across the entire range. This close correspondence suggests consistency in both the angular dependence and underlying collision dynamics of the ionization process. Additionally, the current direct, FB, and positron results all show a peak at 45 degrees, which is consistent with the findings of Jakha *et al*. [21], although the magnitudes of the peaks differ. While the angular positions of the peaks align, their magnitudes vary, likely due to differences in the interaction dynamics and the transition matrix elements used in each model. At high energies, the positron's trajectory is minimally impacted by nuclear repulsion, enabling it to penetrate the electron cloud efficiently. This leads to significantly enhanced energy transfer and ionization, resulting in a definitively higher Triple Differential Cross Section (TDCS) for positrons at high energies.

©2006-2026 Asian Research Publishing Network (ARPN). All rights reserved.

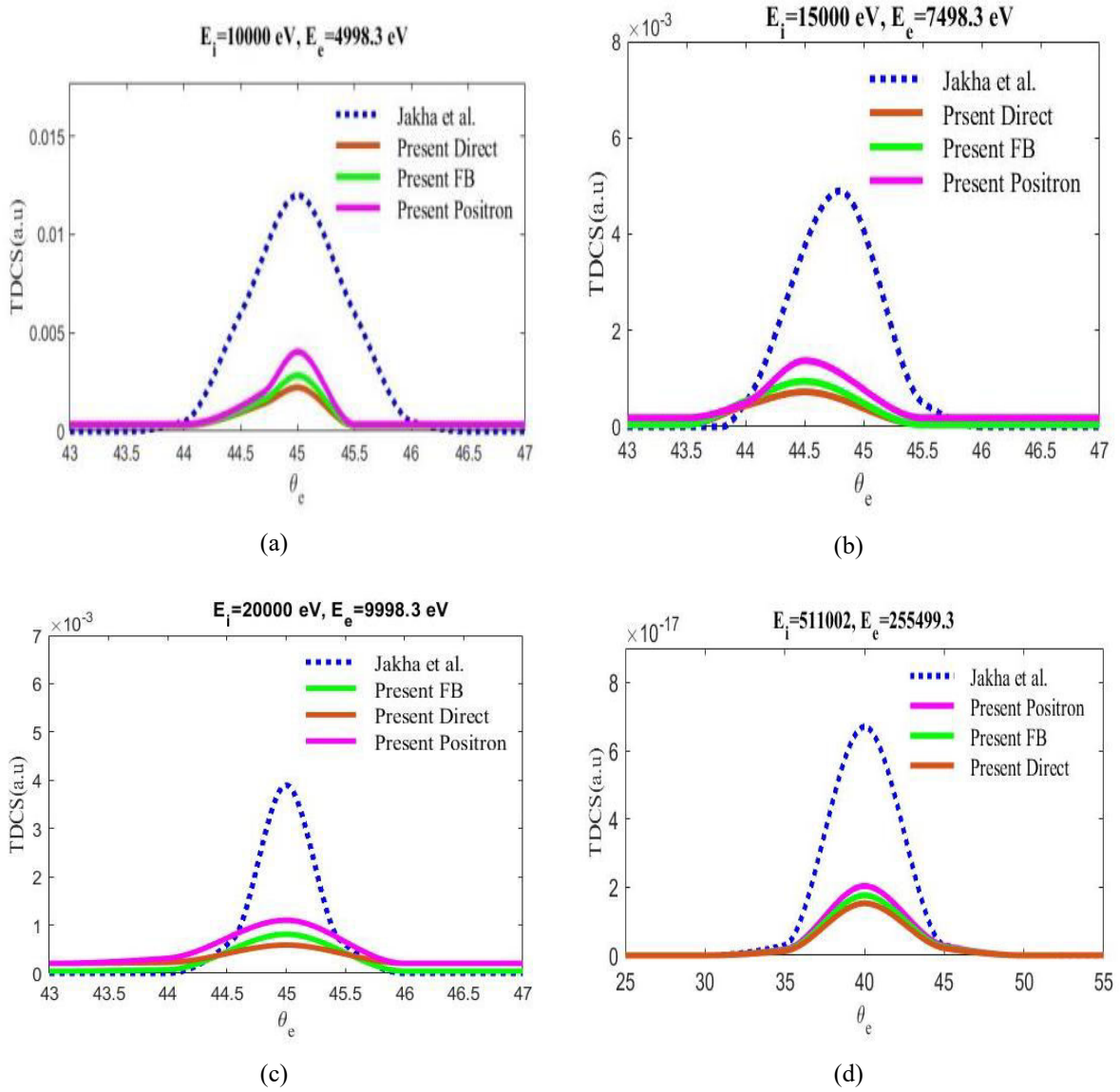


Figure-4. Same as Fig. 3, but at (a) E_i = 10000eV, E_e = 4998.3eV (b) E_i= 15000eV, E_e = 7498.3eV, (c) E_i = 20000eV, E_e = 9998.3eV and (d) E_i = 511002eV, E_e = 255499.3eV.

3.1 Ionization Mechanism

Four different scattering amplitudes, which correspond to distinct terms of the scattering state wave function $\Psi_f^{(-)}(\bar{r}_{ae},\bar{r}_{pe})$ from equation (15), are being considered. In equation (15), for f_{PWB}, $\Psi_f^{(-)}(\bar{r}_{ae},\bar{r}_{pe})$ is given by $e^{i\bar{k}_1.\bar{r}_{ae}+i\bar{k}_2.\bar{r}_{pe}}$ corresponding to the final two particles represented by plane waves. For f_{eT}, $\Psi_f^{(-)}(\bar{r}_{ae},\bar{r}_{pe})=\varphi_{k_1}^{(-)}(\bar{r}_{ae})e^{i\bar{k}_2.\bar{r}_{pe}}$ which is the first Born amplitude, corresponding to a plane wave for the scattered electron and a Coulomb wave for the ejected electron. The amplitude f_{PT}, $\Psi_f^{(-)}(\bar{r}_{ae},\bar{r}_{pe})=\varphi_{k_2}^{(-)}(\bar{r}_{pe})e^{i\bar{k}_1.\bar{r}_{ae}}$ shares similarities with the first Born amplitude , with the exception that the roles of the electron and projectile are interchanged. For f_{Pe}, $\Psi_f^{(-)}(\bar{r}_{ae},\bar{r}_{pe})$is given by $\varphi_{\bar{k}}^{(-)}(\bar{r})e^{i\bar{K}.\bar{R}}$, This term represents the projectile-electron interaction being accurately treated in the final channel, where the center of mass moves as a plane wave. Please see Table-1 to understand the ionization mechanism of four scattering amplitude.

The current form of the scattering amplitude is an effective tool for understanding and predicting scattering outcomes. To gain insight into the scattering mechanism, we analyze the various components of the scattering amplitude across the entire angular region, as outlined in the table, for a specific case. We note that, f_{eT} (f_B), f_{Pe} are large compared to f_{PT} and f_{PWB} in magnitude. The amplitude of the First Born amplitude f_{eT} is higher than

©2006-2026 Asian Research Publishing Network (ARPN). All rights reserved.

that of the higher-order born approximations because it represents the simplest and most probable scattering event, just a single interaction between the projectile and the target. Higher-order Born terms, which represent more complex interactions involving multiple scattering. At high energies, the First Born amplitude f_{eT} tends to dominate because the interaction time is short, and the likelihood of multiple scattering is reduced. Due to its thorough accounting of the projectile-electron interaction in the final state, the amplitude of f_{Pe} is likewise bigger than the f_{PT} and f_{PWB} approximations. In this regime, the FB and f_{Pe} can provide a relatively good approximation of the scattering amplitude.

Table-1. Symmetric H(2S) result for $E_i = 4250$ eV $E_e = 2123.3$ eV

θ_e	f_{eT}		f_{PT}		f_{Pe}		f_{PWB}
40	0.1000 E-10	-0.1000 E-10i	0.3910 E-09	0.2000 E-09i	0.1380 E-08	-0.4650 E-09i	0.6250 E-10
41	0.0000 E-07	-0.0000 E-07i	0.3260 E-09	0.1020 E-09i	0.1567 E-08	-0.1199 E-08i	-0.2287 E-09
42	0.0000 E-07	-0.0000 E-07i	0.3180 E-09	0.8900 E-10i	0.7010 E-09	-0.6670 E-09i	-0.2364 E-09
43	0.0000 E-07	-0.0000 E-07i	0.3360 E-09	0.1170 E-09i	0.1200 E-10	0.2820 E-09i	-0.6150 E-10
44	-0.2700 E-08	-0.2500 E-09i	0.4590 E-09	0.3050 E-09i	0.6000 E-10	0.3268 E-08i	-0.1823 E-09
45	0.1353 E-07	-0.2299 E-07i	0.1823 E-08	0.2399 E-08i	0.4280 E-09	0.3813 E-08i	-0.7843 E-09
46	0.3000 E-10	-0.3000 E-10i	0.4480 E-09	0.2890 E-09i	0.1161 E-08	0.2000 E-10i	-0.1850 E-10
47	0.0000 E-07	-0.0000 E-07i	0.3350 E-09	0.1150 E-09i	0.1640 E-08	-0.9720 E-09i	-0.1754 E-09
48	0.0000 E-07	-0.0000 E-07i	0.3180 E-09	0.8800 E-10i	0.9940 E-09	-0.1021 E-08i	-0.2690 E-09
49	0.0000 E-07	-0.0000 E-07i	0.3270 E-09	0.1030 E-09i	0.1230 E-09	0.1030 E-09i	-0.1035 E-09
50	-0.1100 E-09	0.9000 E-10i	0.3960 E-11	0.2090 E-10i	-0.3000 E-11	0.6690 E-09i	0.2220 E-10

3.2 Proposed Future Research Directions

The TDCS of metastable 2S state hydrogen atoms have not been theoretically assessed for relativistic purposes. As a result, experimental data on the ionization of H (2S) will be valuable. Our findings will contribute a new dimension to this field of study, both from a theoretical and experimental perspective. Further research on total, single, and double differential cross sections using the same wave function across different atoms by electrons and positrons, for both non-relativistic and relativistic atomic ionization, would be valuable. Future experimental setups focusing on hydrogen targets prepared in the 2S metastable state, potentially using atomic beam methods or laser excitation, may offer a practical pathway for direct comparison with theoretical predictions. Such experimental validation would not only test the relativistic formalism but also enhance our understanding of fundamental projectile-target interactions projectile-target interactions.

4. CONCLUSIONS

In this work, the TDCS of atomic hydrogen ionization by the relativistic electron effect have been calculated for symmetric coplanar geometry. Furthermore, the current calculation is in good accord with the ground-state experimental measurement. The new theoretical findings might significantly provide many interesting and potential developments in this research field. A similar qualitative trend with the ground state measurement is also reflected in the present work. The current results cannot be compared because there is no experimental data available in the literature for the symmetric TDCS outcomes of the hydrogenic metastable 2s-state ionization process. Current theoretical calculation reveals additional imaginable formations of the cross-section curves. More work on total, single, and double differential cross sections applying the same wave function in different atoms by electrons and positrons for non-relativistic and relativistic atomic ionization will be interesting.

ACKNOWLEDGEMENT

The computational study has been carried out in the Department of Mathematics Simulation Lab, Chittagong University of Engineering and Technology, Chittagong-4349, Bangladesh.

REFERENCES

[1] Kirchner T. and Knudsen H. 2011. Current status of antiproton impact ionization of atoms and molecules: theoretical and experimental perspectives. Journal of Physics B: Atomic, Molecular and Optical Physics. 44: 122001.

[2] Blanco F., Ellis-Gibbings L. and García G. 2016. Screening corrections for the interference contributions to the electron and positron scattering

©2006-2026 Asian Research Publishing Network (ARPN). All rights reserved.

cross sections from polyatomic molecules. Chem. Phys. Lett. 71: 645.

[3] Jin F., Jr. A. B., Döhring B. M., Ebinger B., Müller A. and Schippers S. 2024. Experimental and theoretical total cross sections for single and double ionization of the open-4d-shell ions Xe, Xe, and Xe by electron impact. Eur. Phys. J. D. 78: 68

[4] Jakubassa-Amundsen D. H., Ponomarev V. Y. 2017. Coincident excitation and radiative decay in electron-nucleus collisions. Phys Rev C. 95(2): 024310.

[5] Haque A. K. F., Uddin M. A., Jakubassa-Amundsen D. H., Saha B. C. 2018. Comparative study of ev to GeV electrons and positrons scattering elastically from neutral atoms. J Phys B: At Mol Opt Phys. 51: 175202.

[6] Ratnavelu K., Brunger M. J., Buckman S. J. 2019. Recommended positron scattering cross sections for atomic systems. J Phys Chem Ref Data. 48(2): 023102.

[7] Arretche F., Barp M. V., Scheidt A., Seidel E. P., Tenfen W. 2019. Semi empirical models for flow energy positron scattering by Ar, Kr and Xe. J Phys B: At Mol Opt Phys. 52(21): 215201.

[8] Dapor M. 2020. Transport of energetic electrons in solids: computer simulation with applications to material analysis and characterization. Springer Nature. 271.

[9] Das J. N. and Seal S. 1993. Electron-Hydrogen Atom Ionization Collisions at Intermediate (5I0-20I0) and High (≤20I0) Energies. Physical Review A. 47: 2978.

[10] Das J. N and Seal S. 1994. Multiple scattering calculations of double and single differential cross sections for Ionization of hydrogen atoms by electrons at intermediate energies. Z Phys D Atoms. 31: 167.

[11] Dhar S. 2008. The Energy Spectrum of Scattered Particles in the K-Shell Ionization of Medium Heavy Atoms by Relativistic Electrons and Positrons with Exchange Effects. J. Phys. B at Mol Phys. 41: 155204.

[12] Brauner M., Briggs M. and Klar H. 1991. Structures in differential cross sections for positron impact ionization of hydrogen. J. Phys. B. At. Mol. Opt. Phys. 24: 2227.

[13] Li S., Berakdar J., Zhang S. T. and Chen J. 2005. Laser Assisted (e, 2e) Reaction in One-Electron Atoms and Ions. Journal of Physics B: Atomic, Molecular and Optical Physics. 38: 1291.

[14] Dal Cappello C., Haddadou A., Menas F. and Roy A. C. 2011. The second born approximation for the single and double ionization of atoms by electrons and positrons. J. Phys. B: At. Mol. Opt. Phys. 44: 015204.

[15] Dhar S. and Nahar N. 2014. Ionization of Metastable 2P-State Hydrogen Atoms by Electron Impact for Coplanar Asymmetric Geometry. Open Journal of Microphysics. 4 46-53.

[16] Dhar S. and Nahar N. 2015. Electron Impact Ionization of Metastable 2P-State Hydrogen Atoms in the Coplanar Geometry. Results in Physics. 5: 3-8.

[17] Dhar S. and Nahar N. 2016. Triple differential cross-sections for the ionization of metastable 2P-state hydrogen atoms by electrons with exchange effects. Pramana-J. Phys. 87: 69.

[18] Akter S., Dhar S., Nahar N., Das L. C. 2018. Ionization of metastable 3P state hydrogen atom by electron with exchange effects. Pramana Journal of Physics. 91: 78.

[19] Banerjee S., Dhar S. 2024. First Born Double Differential Cross-Section for Ionization of H (3d) by Incident Electron Impact. Open Journal of Microphysics. 14: 67-77.

[20] Banerjee S., Dhar S. 2019. Ionization of hydrogenic 3d state by electron impact. Open Journal of Microphysics. 9: 29-39.

[21] Jakha M. , Mouslih S., Taj S., Manaut B., Idrisssi M. EI, Hrour E. 2022. Siher: Relativistic electron - impact ionization of hydrogen atom from its metastable 2S-state in the symmetric/asymmetric coplanar geometries. Chin. J. Phys. 77.

[22] Montanari C. C. and Miraglia J. E. 2012. Antiproton, proton and electron impact multiple ionization of rare gases. Journal of Physics B: Atomic, Molecular and Optical Physics. 45: 105201.

[23] Montanari C. C. and Miraglia J. E. 2015. Electron-impact multiple ionization of Ne, Ar, Kr and Xe. Journal of Physics B: Atomic, Molecular and Optical Physics. 47: 105203.

©2006-2026 Asian Research Publishing Network (ARPN). All rights reserved.

[24] Montanari C. C. and Miraglia J. E. 2015. Positron and electron-impact multiple ionization. Journal of Physics B: Atomic, Molecular and Optical Physics. 48: 165203.

[25] Shyn T. W. 1992. Doubly differential cross sections of secondary electrons ejected from atomic hydrogen by electron impact. Phys. Rev. A. 45: 2951.

[26] Ren X., Dorn A. and Ullrich J. 2008. Coulomb Four-Body Problem: Electron-Impact Double Ionization of Helium in the Threshold Regime. Physical Review Letters. 101: 093201

[27] Milisavljevic S., Sevic D., Chauhan R. K., Pejsev V., Filipovic D. M., Srivastava R. and Marinkovic B. P. 2005. Differential and integrated cross sections for the elastic electron scattering by calcium atom. J. Phys. B: At. Mol. Opt. Phys. 38: 2371

[28] Das J. N. and Dhar S. 1998. Energy spectrum of scattered electrons in K-shell ionization of medium to heavy atoms by relativistic electrons. J. Phys. B: At. Mol. Opt. Phys. 31: 2355-2358.

[29] Lewis R. R. 1956. Potential scattering of high-energy electrons in second born approximation. Physical Review. 102: 537.

[30] Sakurai J. J. and Napolitano Jim. 2021. Modern Quantum Mechanics. Cambridge University Press.